Supporting Information for

Dynamic Self-Rectifying Liquid Metal-Semiconductor Heterointerfaces: A Platform for Development of Bio-Inspired Afferent Systems

Mohammad Karbalaei Akbari, [1,2] Serge Zhuiykov [1,2]*

[1] Department of Solid State Sciences, Faculty of Science, Ghent University, 9000 Ghent, Belgium. Email: Mohammad.akbari@Ugent.be; Serge.Zhuiykov@Ugent.be
[2] Centre for Environmental & Energy Research, Faculty of Bioscience Engineering, Ghent University, Global Campus, Incheon, South Korea.

Mohammad Karbalaei Akbari: ORCID ID: 0000-0001-9367-8475
Serge Zhuiykov: ORCID ID: 0000-0003-2709-1259

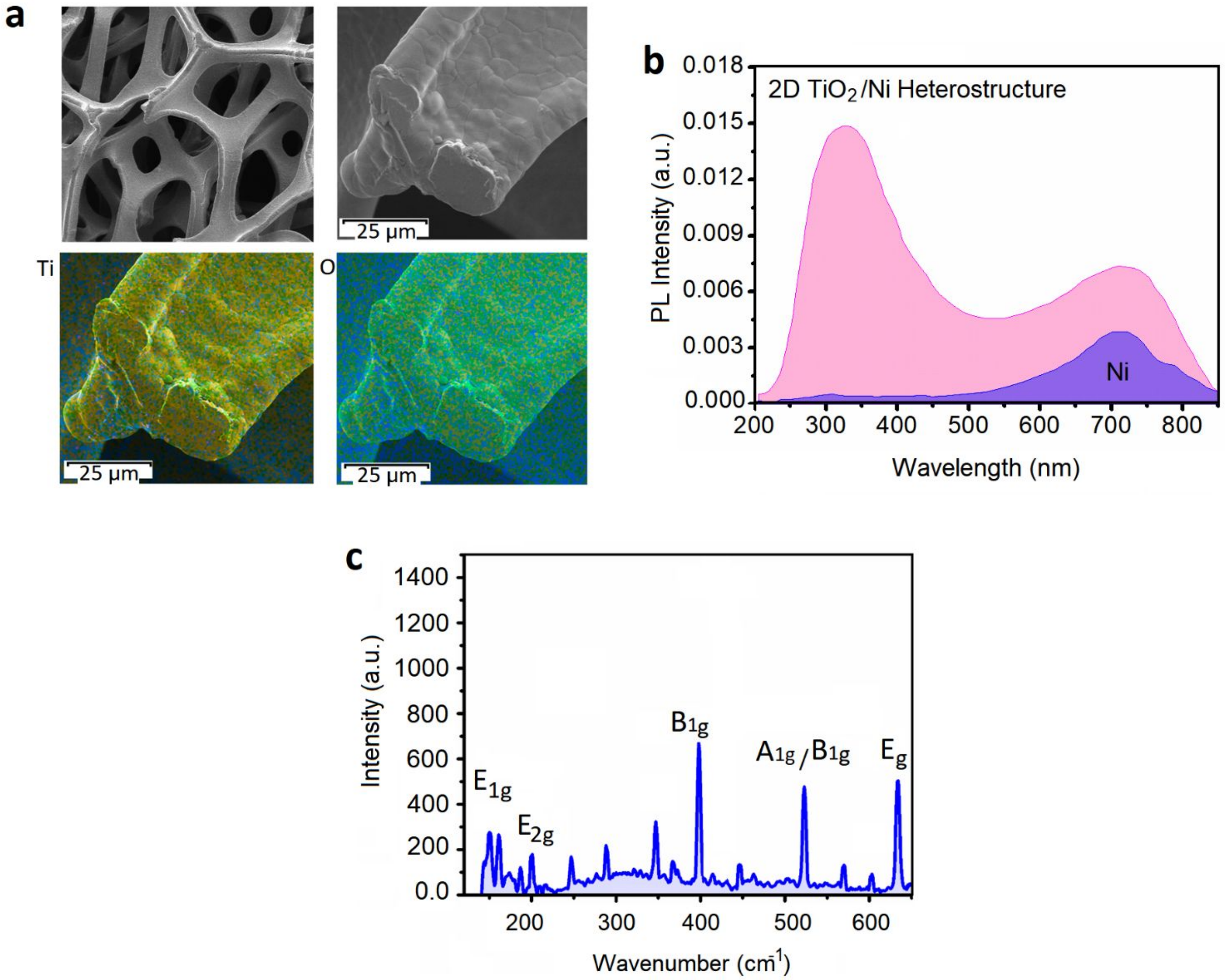

Figure S1. Characterization of 3D network of ultra-thin TiO_2/Ni heterojunction. (a) SEM and following EDS map of the structural elements of TiO_2/Ni heterojunction. (b) The photoluminescence (PL) and (c) Raman vibration peaks of TiO_2/Ni heterojunction.

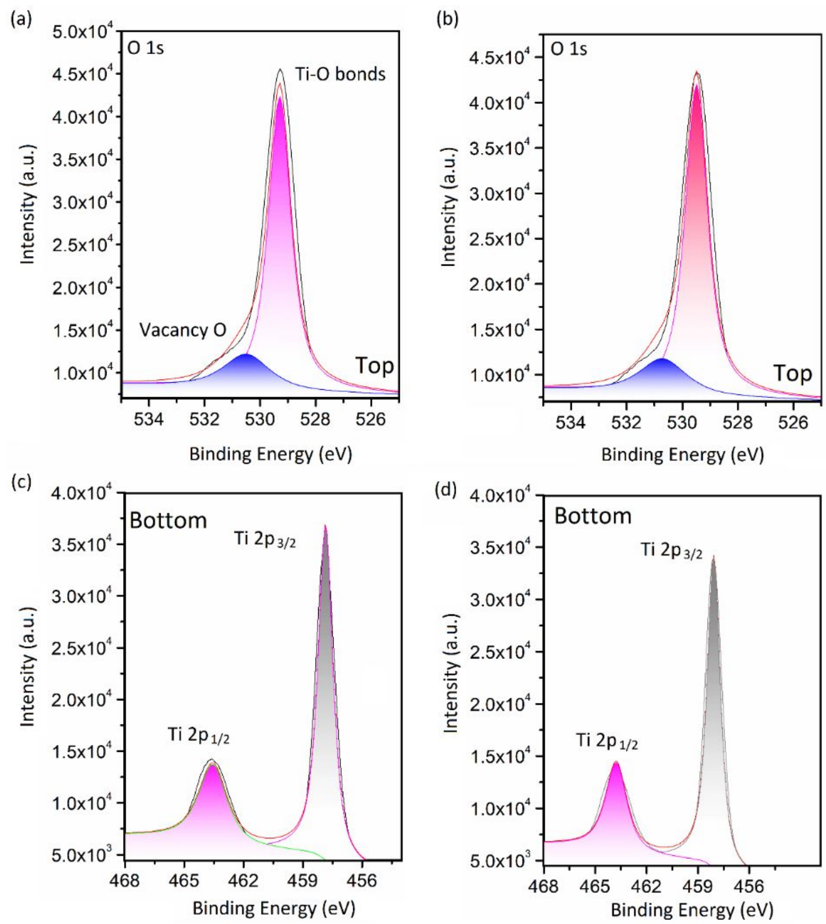

Figure S2. **a** The O 1s XPS peak of TiO_2 film on uppermost and **b** bottom part of TiO_2/Ni 3D network. **c** The Ti 2p XSP peak of the top and **d** bottom part of samples.

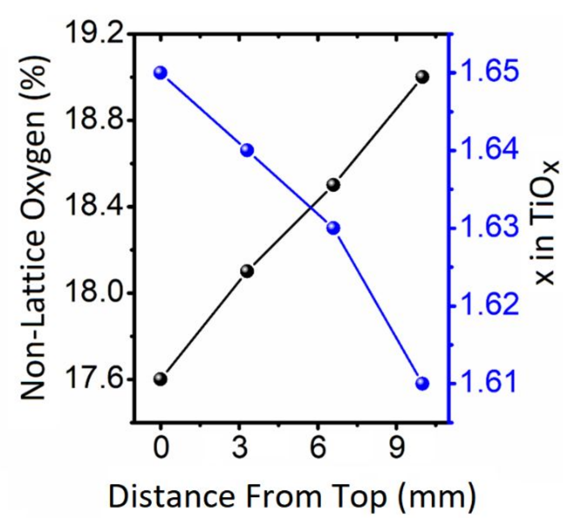

Figure S3. The quantitative analysis of percentage of lattice and non-lattice oxygen of TiO_2/Ni heterostructure at different distances from the top section to the bottom part of TiO_2/Ni 3D foam.

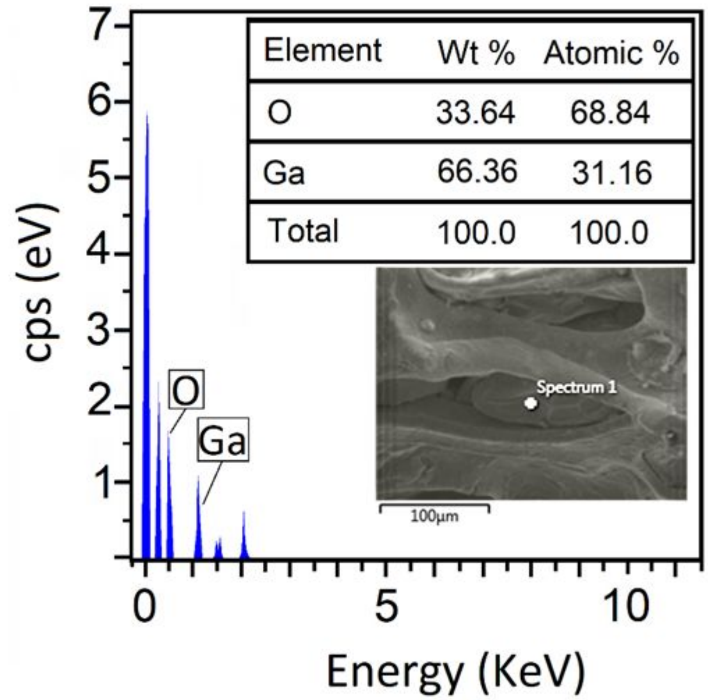

Figure S4. The EDS analysis of surface oxide film of galinstan at EGaInSn/Ga_2O_3-TiO_2/Ni heterointerfaces.

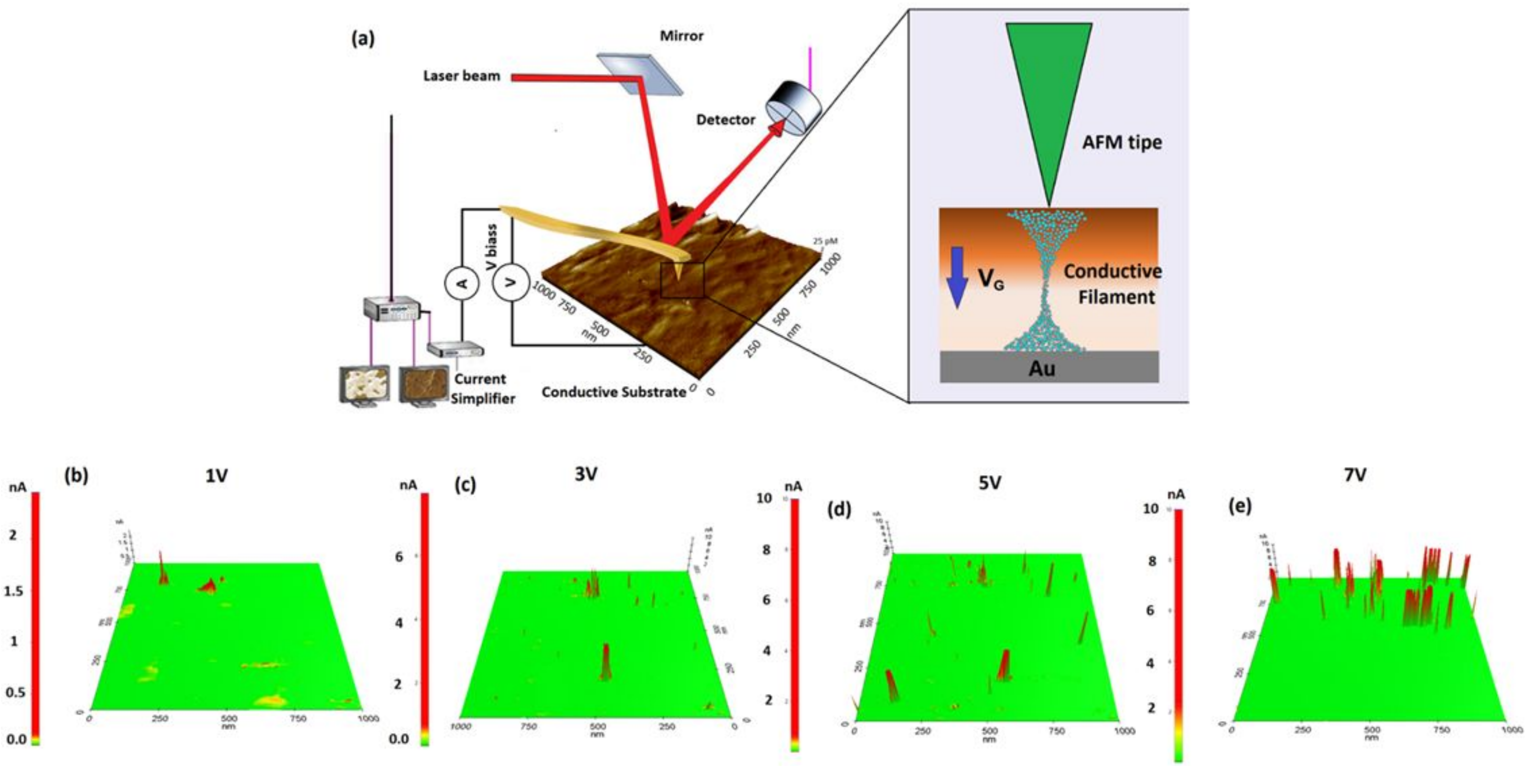

Figure S5. The measurement of resistive switching characteristics of 6.0 nm thick TiO_2 film on Ni substrate by c-AFM**. a** The working principles of c-AFM is based on the formation of conductive filament between the AFM tip and under layer Ni substrate. **b, c, d** ,and **e** respectively show the current maps of TiO_2 film captured under 1.0, 3.0, 5.0 and 7 V potential.

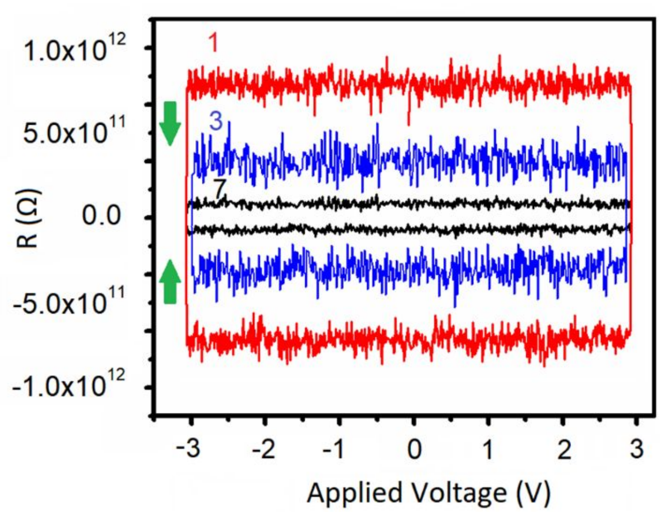

Figure S6. The variation of resistance of 6.0 nm thick TiO_2 film collected via c-AFM at different *I-V* cycles.

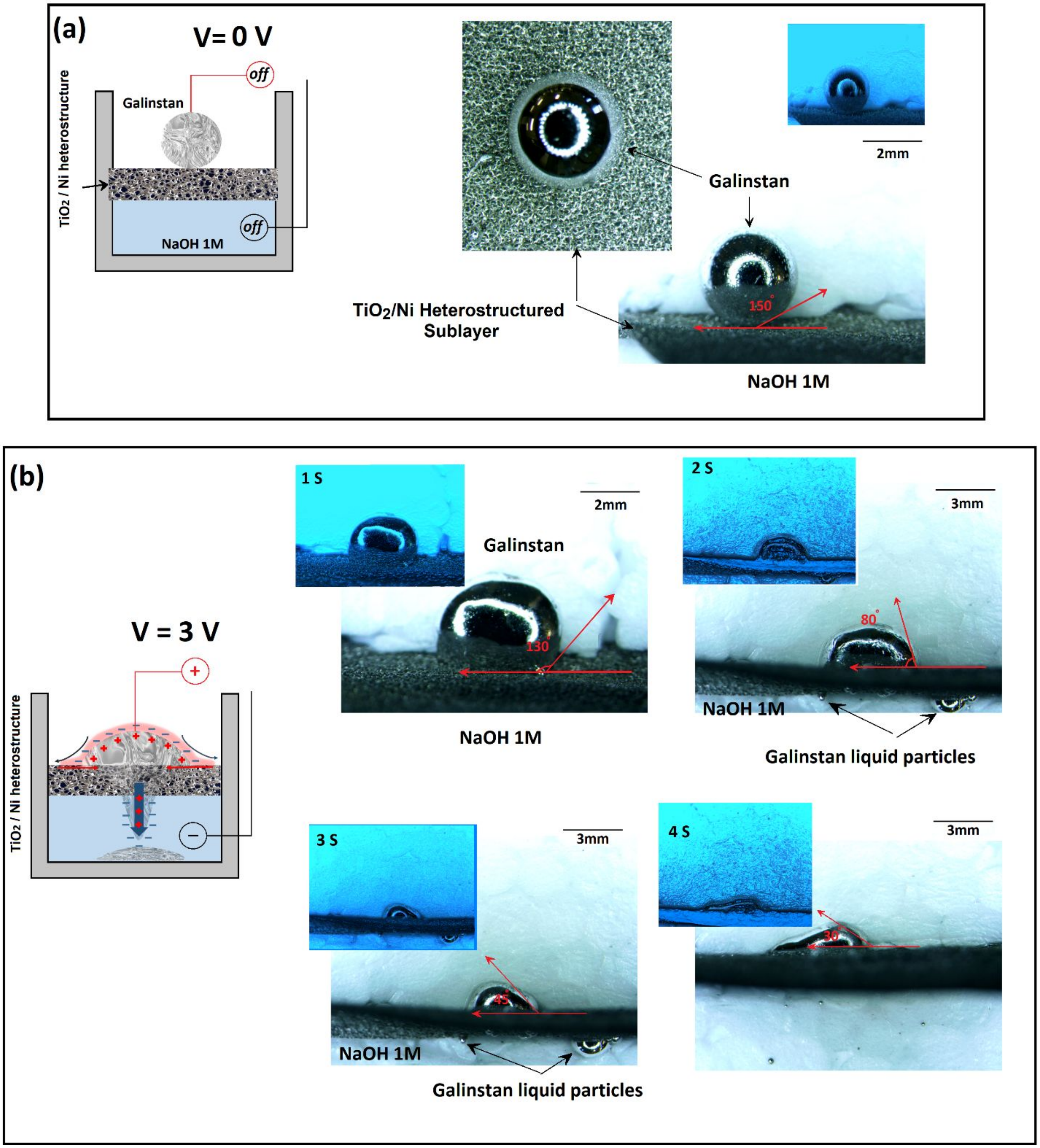

Figure S7. Schematic diagram and snapshots of spreading and penetration of liquid galinstan into porous TiO_2/Ni sublayer. **a** When the applied voltage is 0.0 V, the galinstan droplet is in fully hydrophobic state. **b** When +3.0 V constant driving force is applied on the galinstan droplet, it starts spreading on the surface of TiO_2/Ni 3D network. The optical and fluorescence images depicting the snapshot of penetration of galinstan into TiO_2/Ni 3D network.

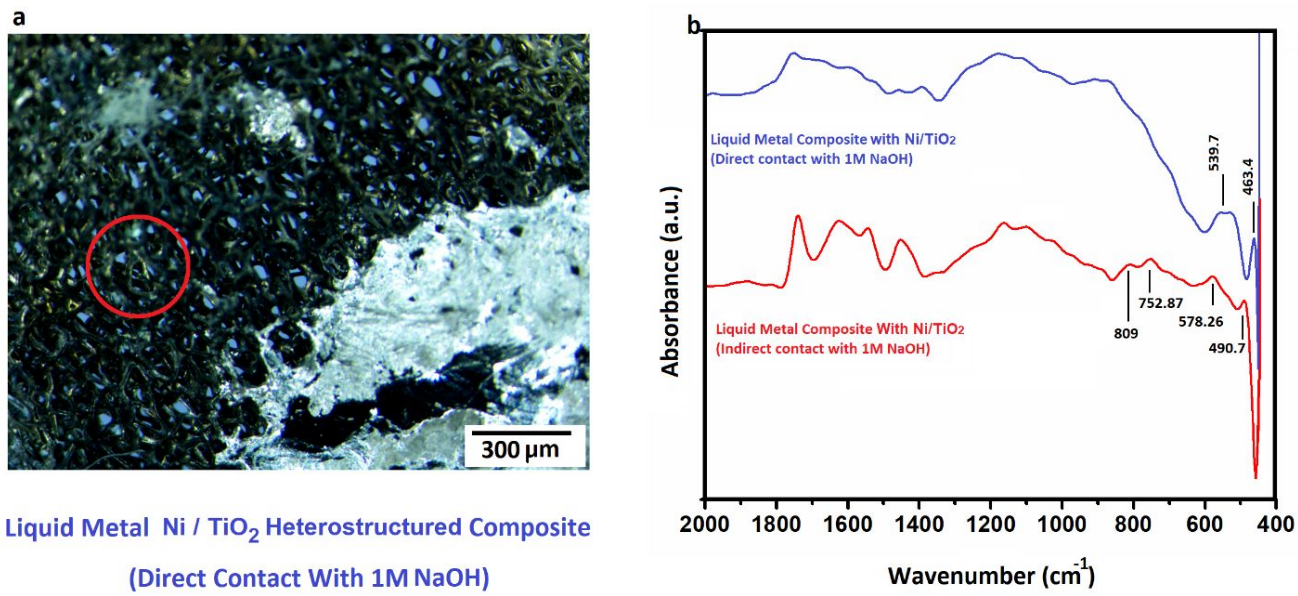

Figure S8. **a** The sedimentation of NaGa(OH) on the surface of porous TiO_2/Ni heterostructured layer, and **b** it's corresponding FTIR characteristic peaks depicting the formation of gallat compounds on the surface.

Supplementary Note 1:

The penetration of liquids into porous structure depends on the viscosity and surface tension of them. Without applying an external voltage, the surface tension is still high, thus the galinstan (EGaInSn) droplet keeps its ultimate spherical shape on the surface of TiO_2/Ni foam (Figure S7). Upon application of external voltage (+3.0 V) on EGaInSn droplet, and due to the influence of external electric filed, the significant decrease in the surface tension occurs. It results in the sudden drop of wettability angle within few seconds (Figures 3b). The decrease of surface tension, accompanied by the high density of EGaInSn (6.35 gr/cm^3) contribute to overcome the viscosity and friction forces. Another problem arises from the direct and uncontrolled contact of EGaInSn by NaOH solution which resulted in the deposition of gallat compounds (similar to NaGaOH) on the surface of TiO_2-Ni 3D network (Figure S8). To tackle these challenges a polyurethane membrane (10 µm pore size) was employed in NaOH bath to restrict the number of contact points between NaOH and EGaInSn droplet to few limited drift channels. The diameter of EGaInSn channels are in the range of 10 µm. The number and the size of these channels are restricted, thus the impregnation time would be considerably longer than that of direct contact method. Usually the first appearance of EGaInSn alloy on the bottom side of TiO_2/Ni 3D network was observed after 5 s of employment of +3 V driving force (Figure S9). Figure S9b demonstrates the down view of impregnation stage where the first EGaInSn droplets successfully penetrated and passed through the TiO_2/Ni 3D network. After 5 s the impregnation is finalized and the EGaInSn was successfully impregnated inside of TiO_2/Ni 3D network and covered 5x5 mm^2 area of surface (Figure S9b).

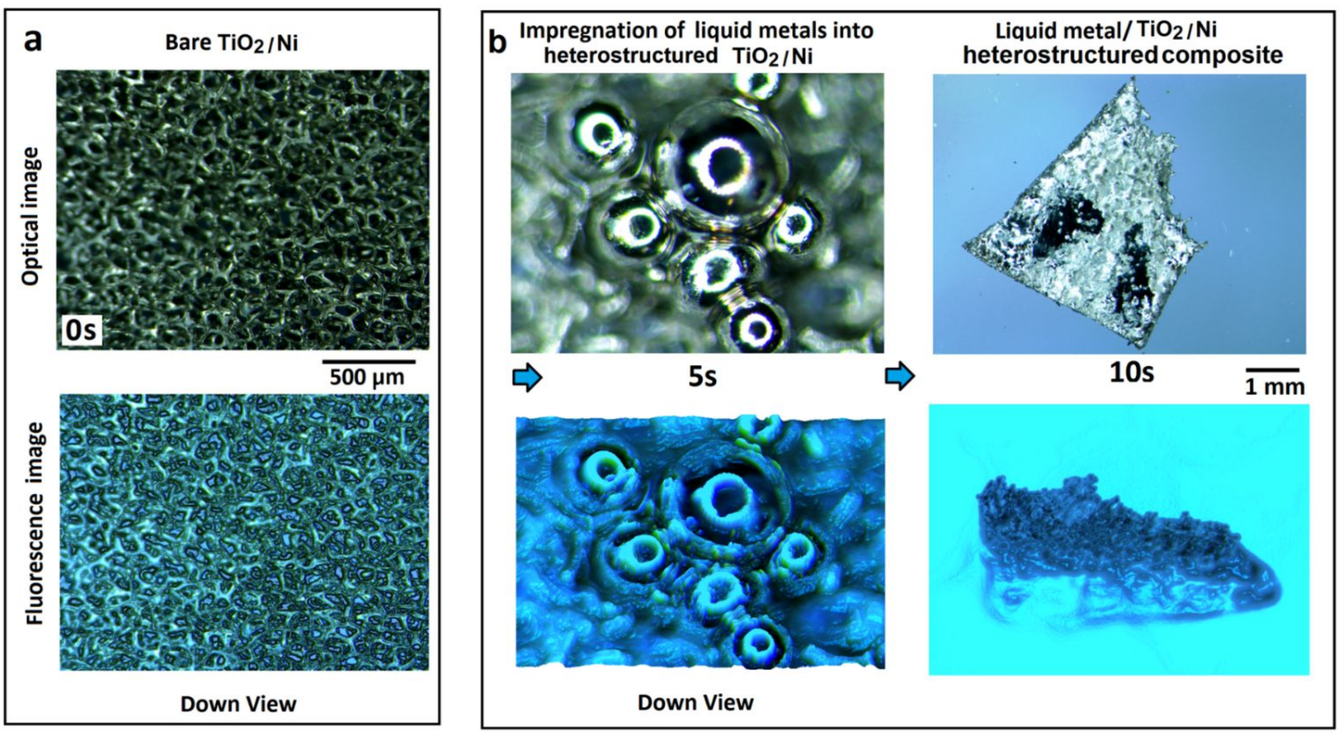

Figure S9. **a** The optical image and its corresponding fluorescence image from bottom of TiO_2/Ni 3D network before the start of impregnation. **b** The penetration of galinstan into TiO_2/Ni 3D network by applying voltage. The optical and fluorescence images depicting the snapshot of penetration of EGaInSn into TiO_2/Ni 3D network.

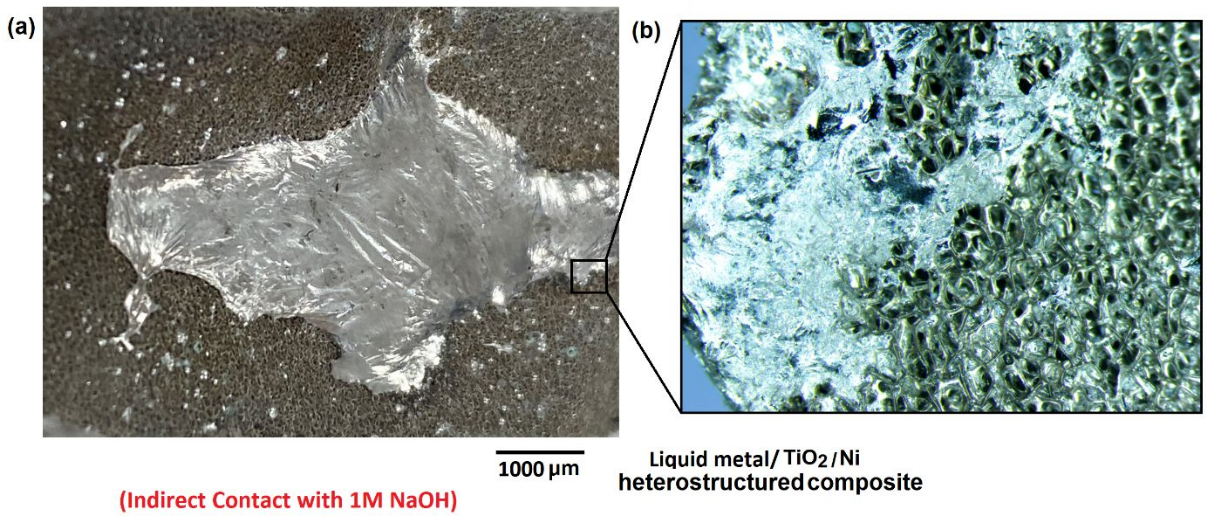

Figure S10. **a** The low magnification and **b** high magnification images of impregnated EGaInSn into TiO_2/Ni 3D network.

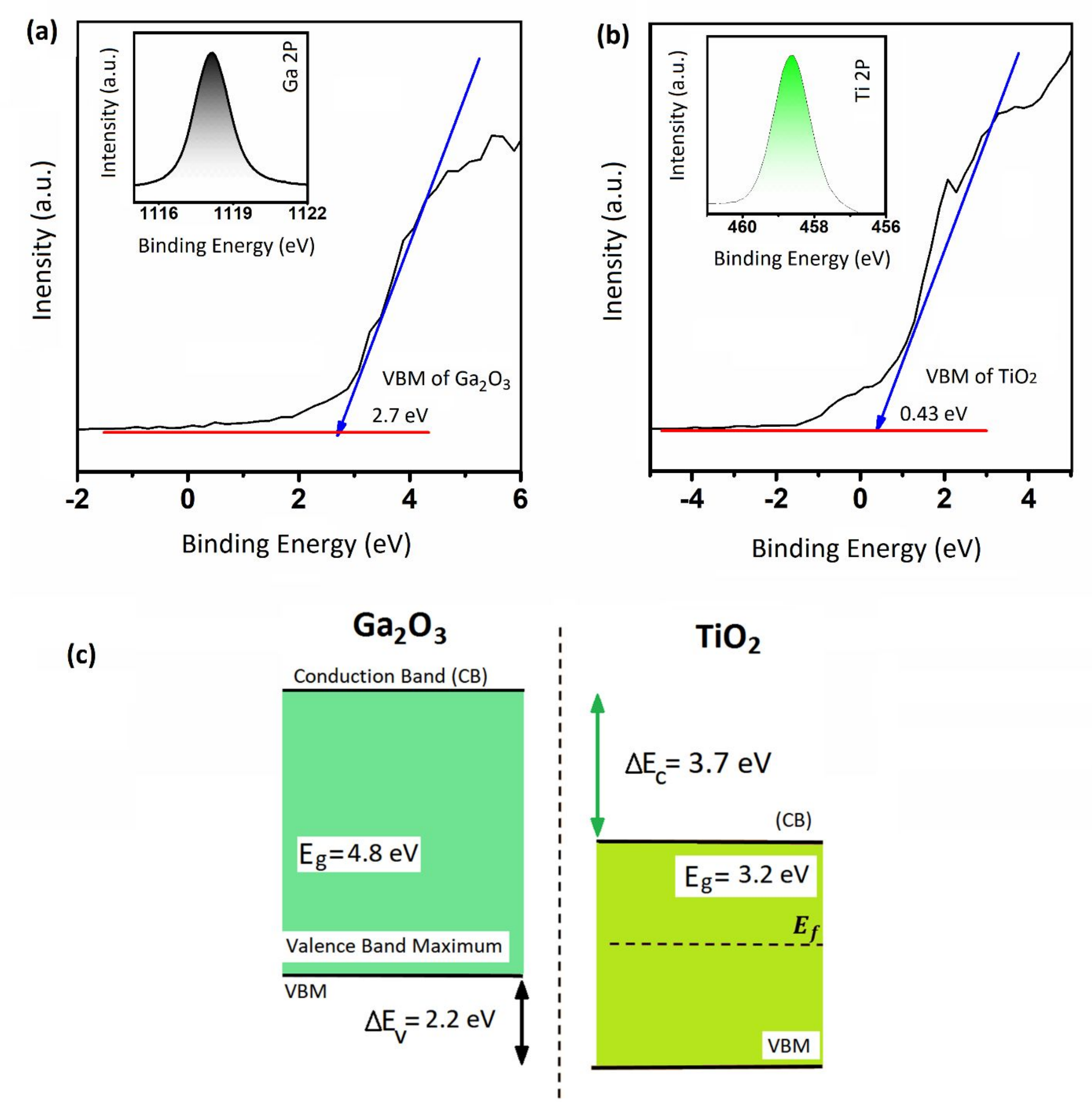

Figure S11. The energy band alignment at Ga_2O_3-TiO_2 heterojunction calculated by Kraut's method. **a** The valence band maximum (VBM) of Ga_2O_3 surface oxide film. (Inset shows the Ga 2p peak of Ga_2O_3). **b** The VBM of TiO_2 . (Inset shows the Ti 2p peak of TiO_2). **c** The energy bandalignment at Ga_2O_3-TiO_2 heterojunction.

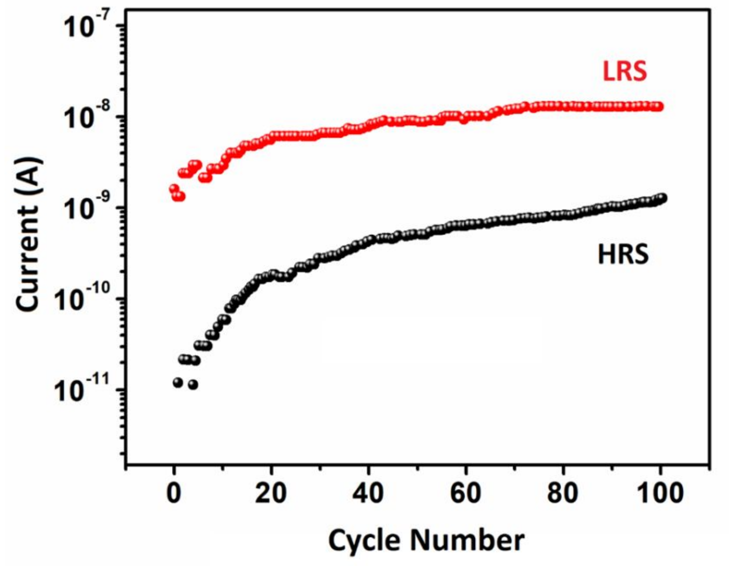

Figure S12. The cycle-to-cycle resistive switching characteristics of dynamic EGaInSn/Ga_2O_3-TiO_2/Ni heterostructure**.**

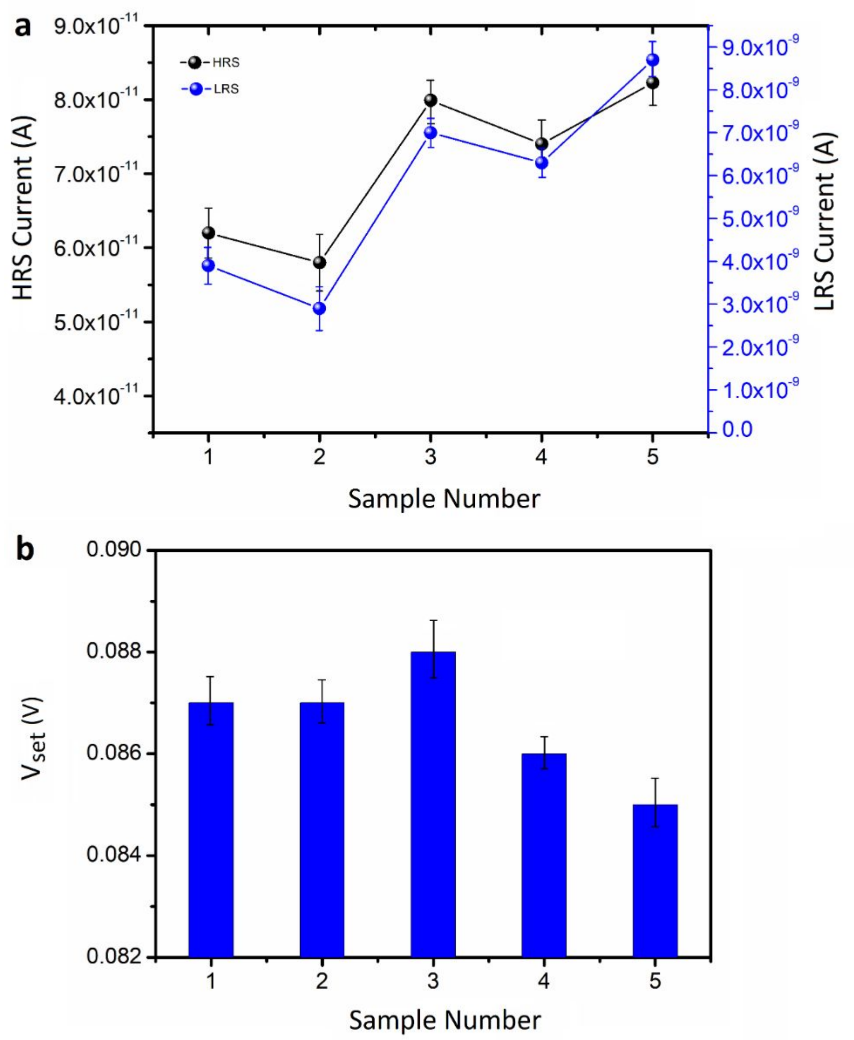

Figure S13. The device-to-device resistive switching characteristics of dynamic EGaInSn/Ga_2O_3-TiO_2/Ni heterostructure. **a** The variation of HRS and LRS currents of five individual devices. **b** The variation of V_{set} of five individual devices at their 10th resistive switching cycle.